Role of band 3 in regulating metabolic flux of red blood cells

Ian A. Lewis[a], M. Estela Campanella[b], John L. Markley[a], and Philip S. Low[b,1]

[a]Department of Biochemistry, University of Wisconsin, 433 Babcock Drive, Madison WI 53706; and [b]Department of Chemistry, Purdue University, 560 Oval Drive, West Lafayette, IN 47907

Edited by Vincent T. Marchesi, Yale University School of Medicine, New Haven, CT, and approved September 17, 2009 (received for review May 29, 2009)

Deoxygenation elevates glycolytic flux and lowers pentose phosphate pathway (PPP) activity in mammalian erythrocytes. The membrane anion transport protein (band 3 or AE1) is thought to facilitate this process by binding glycolytic enzymes (GEs) and inhibiting their activity in an oxygen-dependent manner. However, this regulatory mechanism has not been demonstrated under physiological conditions. In this study, we introduce a ^{1}H-^{13}C NMR technique for measuring metabolic fluxes in intact cells. The role of band 3 in mediating the oxygenated/deoxygenated metabolic transition was examined by treating cells with pervanadate, a reagent that prevents the GE–band 3 complex from forming. We report that pervanadate suppresses oxygen-dependent changes in glycolytic and PPP fluxes. Moreover, these metabolic alterations were not attributable to modulation of bisphosphoglycerate mutase, direct inhibition of GEs by pervanadate, or oxidation, which are the major side effects of pervanadate treatment. These data provide direct evidence supporting the role of band 3 in mediating oxygen-regulated metabolic transitions.

erythrocyte | glycolysis | pervanadate | NMR

Human erythrocytes circulate between the lungs and peripheral tissues approximately every minute, exposing the cells to rapidly changing metabolic demands (1). In the lungs, where O_2 partial pressures are high, erythrocytes are exposed to oxidative stresses that must be controlled by accelerated production of reducing equivalents derived from the pentose phosphate pathway (PPP). In the peripheral tissues, where O_2 pressures are low, erythrocytes must pass through capillaries much smaller than their own diameters (2), causing the cells to distort as they flow from the arterioles to the postcapillary venules. The resulting mechanical stresses induce cation leaks (3) that create an enhanced demand for glycolytically derived ATP to restore intracellular ion balances. Several layers of metabolic regulation allow erythrocytes to match ATP, NADH, and NADPH production with fluctuations in oxidative stress and ion leakage. One of these mechanisms is oxygen-dependent control of glycolytic and PPP activity.

Historically, oxygen-dependent metabolic regulation has been attributed to alterations in pH, classical allosteric mechanisms, and demand for ATP (4–8). However, experimental evidence indicates that these metabolic regulators operate independently from oxygen tension (9), suggesting that the models are incomplete. An alternative mechanism, which is supported by a growing body of evidence, argues that erythrocyte metabolism is regulated through the oxygen-dependent assembly of glycolytic enzymes (GEs) into inhibitory complexes on the membrane anion exchange protein (band 3 or AE1). Although several lines of indirect evidence support this hypothesis, the GE–band 3 model has not been demonstrated in intact cells.

Early evidence for band 3-dependent glycolytic regulation was derived from in vitro binding assays, which showed that purified fragments of the membrane anion exchange protein (band 3 or AE1) interact with several GEs (10–13). Although debate subsequently emerged over the in vivo significance of these data (14), it is now clear that phosphofructokinase, aldolase, and GAPDH bind to band 3 in intact cells (15). A variety of band 3-specific perturbations have been shown to disrupt the GE–band 3 interaction; GEs are readily displaced from the membrane by antibodies to the amino terminus of band 3 and by phosphorylation of band 3's tyrosine residues (15). Furthermore, peptide fragments of band 3's GE binding site compete with native band 3 for GEs in resealed cells (16), and transgenic mice lacking band 3 exhibit no membrane-associated GEs (16).

Several indirect lines of evidence suggest that GE–band 3 interactions act as an oxygen-dependent metabolic regulator. Whereas oxyHb has no affinity for band 3, deoxyHb binds to the GE site on band 3 with high affinity (17). Consequently, competition between deoxyHb and GEs causes GEs to be released from membrane upon deoxygenation (15). Deoxygenation also triggers higher glycolytic flux and reduced PPP activity in intact erythrocytes (18–21). This observation is significant in that purified fragments of band 3's cytoplasmic tail reduce the in vitro catalytic activity of GEs (10–12). Together, these studies suggest that the lower glycolytic fluxes observed in oxygenated erythrocytes result from catalytic inhibition of GEs via the GE–band 3 interaction, whereas elevated glycolytic fluxes of deoxygenated erythrocytes result from deoxyHb displacing GEs from their inhibitory site on band 3.

Although the GE–band 3 model is commonly used to explain oxygen-dependent metabolic phenomena in RBCs (22), the model has not been convincingly demonstrated in intact cells. To date, only two publications have tested the band 3 model directly. The first, by Messana et al. (19), showed that red cells treated with 4,4′-diisothiocyanatostilbene-2,2′-disulfonic acid (DIDS), a covalent inhibitor of band 3-mediated anion transport, exhibit altered PPP activity. However, Messana et al.'s study did not demonstrate any effect of DIDS on GE–band 3 interactions nor did it control for the effects of DIDS on intracellular pH, membrane skeletal interactions (23), or ion concentrations. The second article, by Kinoshita et al. (24), showed that computer models of red cell metabolism are consistent with band 3-mediated metabolic regulation (24), but it provided limited experimental evidence to support their computations.

In this study, we introduce a ^{1}H–^{13}C NMR technique for quantifying metabolic pathway flux in intact cells. We examine the metabolic consequences of disrupting the GE–band 3 interaction in intact cells by stimulating tyrosine phosphorylation on band 3 with pervanadate. Pervanadate disrupts the GE complex by inducing phosphorylation of the two tyrosines (Y8 and Y21) that are located within the GE binding site on band 3 (25, 26). We report that oxygenated RBCs treated with pervanadate have increased glycolytic flux, reduced pentose shunt activity, and are metabolically

Author contributions: I.A.L., M.E.C., J.L.M., and P.S.L. designed research; I.A.L. and M.E.C. performed research; I.A.L., M.E.C., J.L.M., and P.S.L. analyzed data; and I.A.L., M.E.C., J.L.M., and P.S.L. wrote the paper.

The authors declare no conflict of interest.

This article is a PNAS Direct Submission.

[1]To whom correspondence should be addressed. E-mail: plow@purdue.edu.

This article contains supporting information online at www.pnas.org/cgi/content/full/0905999106/DCSupplemental.

BIOCHEMISTRY

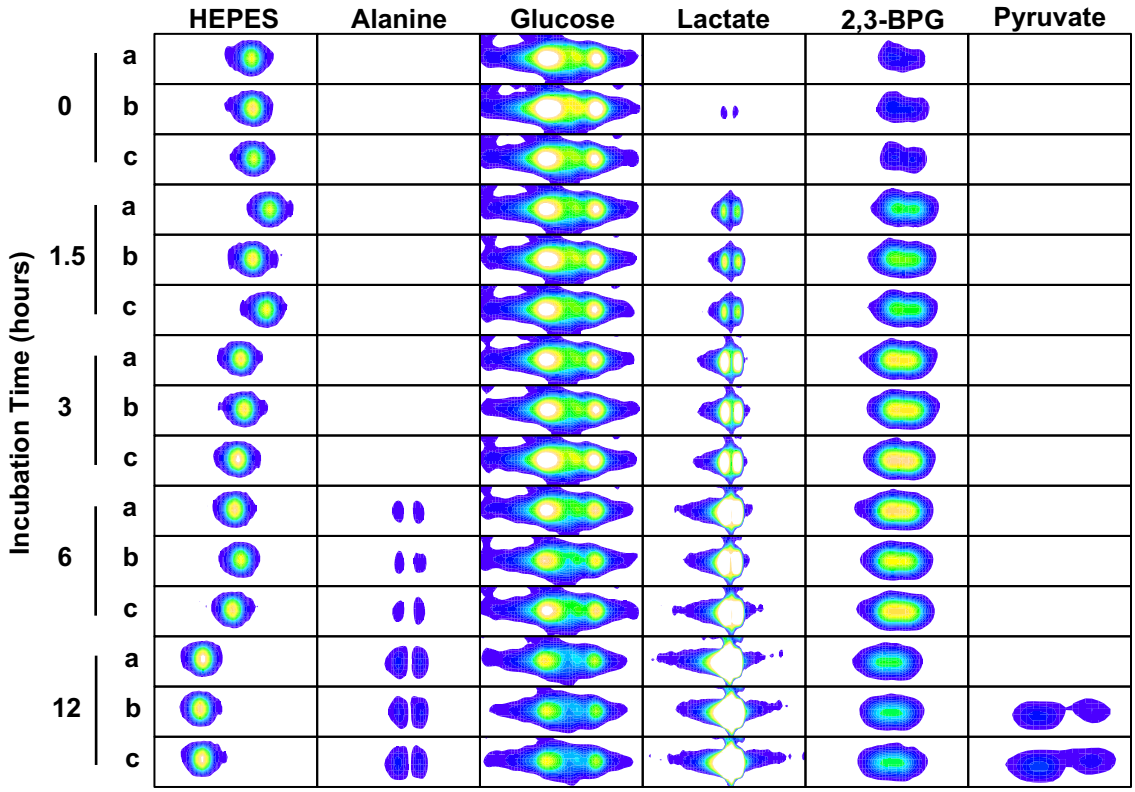

Fig. 1. 2D ^{1}H-^{13}C HSQC NMR spectra of three (a, b, and c) erythrocyte samples. Each box shows an NMR cross-peak of a metabolite observed in untreated samples incubated in U-^{13}C glucose over a 12-h time course. The minimum and maximum cross-peak contours shown in each spectrum depict signal intensities between 6 and 20 SD above the thermal noise threshold.

unresponsive to deoxygenation. These findings are consistent with the band 3-mediated metabolic regulatory model and suggest that the GE–band 3 complex plays a direct role in regulating glycolytic and pentose shunt fluxes of intact erythrocytes.

Results

We hypothesized that pervanadate-induced disruption of the GE–band 3 complex would stimulate glycolytic flux in oxygenated RBCs and prevent cells from responding metabolically to changes in oxygen tension. To test this hypothesis, we incubated pervanadate-treated erythrocyte suspensions in isotopically enriched glucose and measured the concentrations of isotopically enriched metabolites over a 12-h time course. Oxygen-dependent metabolic regulation was monitored by conducting the isotopic labeling experiments under both oxygenated and deoxygenated conditions. Concentrations of ^{13}C-labeled metabolites were measured by ^{1}H and ^{1}H-^{13}C NMR (Fig. 1), and metabolic fluxes were calculated by regressing observed concentrations as a function of incubation time (Fig. 2 and Table 1).

Untreated erythrocytes were used to validate our analytical technique and served as a negative control for pervanadate treatment. As has been shown elsewhere (21), glycolytic fluxes of untreated controls differed significantly between oxygenated and deoxygenated conditions. Deoxygenated controls showed higher rates of glucose uptake, 2,3-bisphosphoglycerate (2,3-BPG) flux, lactate production, and pH change than oxygenated controls (Fig. 2). Overall, glycolytic fluxes of deoxygenated controls were 41% ($P < 0.001$) higher than oxygenated samples. This effect was replicated in two independent pools of blood that were collected and analyzed on different dates. Although some variation in glycolytic fluxes was observed between the two studies, observed kinetics were consistent within the range of values reported in similar studies (19, 21, 27) (Table 1).

In contrast to the normal metabolic responses observed in untreated controls, pervanadate-treated samples showed significant alterations in oxygen-dependent metabolic regulation. Under oxygenated conditions, pervanadate-treated samples showed higher rates of glucose uptake, lactate production, and pH change than untreated controls (Table 1). On average, glycolytic fluxes of pervanadate-treated samples were 45% higher ($P < 0.001$) than their corresponding oxygenated controls. In contrast, rates of glucose uptake and lactate production observed in deoxygenated pervanadate-treated samples did not differ significantly from deoxygenated controls (Fig. 3). The 45% increase in glycolytic flux of oxygenated pervanadate-treated samples, in combination with the negligible alterations to deoxygenated flux, reversed the normal oxygen-dependent metabolic response of red cells. Whereas untreated controls showed higher glycolytic activity under deoxygenated conditions, pervanadate-treated samples were more glycolytically active under oxygenated conditions (Fig. 3).

Band 3-dependent metabolic regulation has primarily been studied in the context of glycolysis. However, glycolytic inhibition by the GE–band 3 complex could stimulate PPP flux by making more substrate available to the pentose shunt (19, 28). To determine the role of the GE–band 3 complex in regulating PPP flux, cell suspensions were incubated with 2-^{13}C-glucose for 12 h. PPP fluxes were calculated from the positional isotopic enrichment of lactate observed in ^{1}H NMR spectra of cell extracts. In accordance with previous studies (18, 19, 21), pentose shunt flux accounted for 6% of total glucose consumption in oxygenated controls, but only 3% in deoxygenated controls (51% decrease; $P = 0.013$; Table 1). As expected, methylene blue, a traditional positive control for pentose shunt stimulation, increased pentose shunt activity to 21% of total incoming glucose ($P < 0.001$ relative to untreated samples).

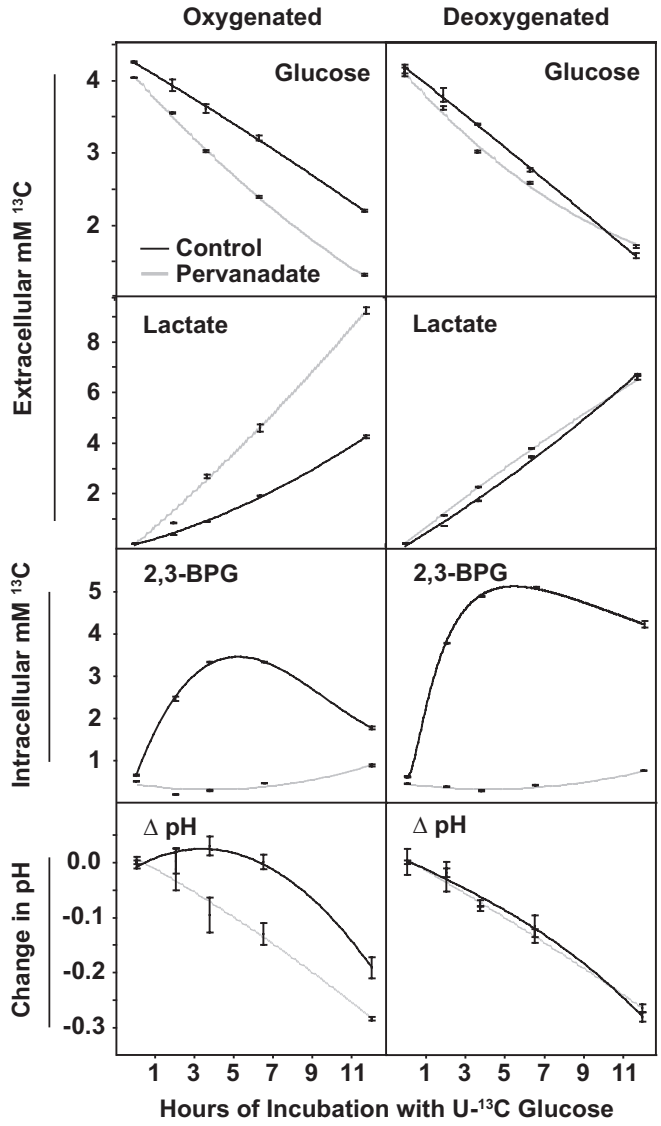

Fig. 2. Concentrations of ^{13}C-labeled metabolites and pH observed in erythrocyte extracts. RBC suspensions (20% hematocrit) were incubated with U-^{13}C-glucose for 12 h, and metabolite concentrations were measured by ^{1}H-^{13}C NMR. Black lines indicate untreated RBCs, gray lines indicate pervanadate-treated RBCs, and error bars show standard error.

We predicted that pervanadate-induced disruption of the GE–band 3 complex would shift metabolic flux toward glycolysis and thus diminish PPP flux under oxygenated conditions. Positional isotopic enrichment data supported this prediction (Fig. 3). Under oxygenated conditions, pervanadate decreased pentose shunt activity by 66% ($P = 0.022$). Similar to the pattern observed in glycolytic fluxes, pervanadate-induced metabolic alterations were most pronounced under oxygenated conditions. Whereas deoxygenation induced a significant ($P = 0.013$) reduction in the PPP activity of control samples, pervanadate-treated samples showed no significant differences ($P = 0.13$) between oxygenated and deoxygenated conditions.

In addition to the metabolic alterations predicted in the GE–band 3 model, pervanadate elicited two detectable side effects: a complete absence of 2,3-BPG and elevated production of pyruvate and alanine. Both pervanadate-induced disappearance of 2,3-BPG and elevated pyruvate production have been previously attributed to phosphatase activity by bisphosphoglycerate mutase (27). Elevated alanine production has not been reported in conjunction with pervanadate treatment, but pyruvate and alanine are readily interconverted via aminotransferases (29). Isotopically enriched pyruvate and alanine were detected in untreated erythrocytes, although observed biosynthetic rates were considerably lower in untreated controls than in pervanadate-treated samples (Table 1). NMR analysis of the incubation medium indicated that these metabolites were accumulating extracellularly (Fig. S1). When expressed as a fraction of total carbon output, pyruvate and alanine accounted for 6% and 2% in oxygenated and deoxygenated controls, respectively. In contrast, the glycolytic side products accounted for 5% of the total carbon output in pervanadate-treated samples, regardless of their oxygenation state.

Enzymatic activity by NADH-dependent methemoglobin reductase is a band 3-independent effect that could contribute to increased glycolytic fluxes observed in pervanadate-treated samples. The mechanism for oxidation of oxyhemoglobin to methemoglobin involves an electron transfer between the heme iron and the bound O_2 (30). CO can be used to inhibit the formation of methemoglobin and thereby suppress demand for NADH-dependent methemoglobin reductase. To control for effects on methemoglobin reductase activity, rates of glucose consumption in pervanadate-treated and untreated samples were measured in washed erythrocytes incubated in CO, air, and argon. Samples incubated in carbon monoxide showed no significant differences in glucose consumption when compared with samples incubated in air (Fig. S2). As expected, glycolytic rates for samples incubated in air and argon matched our previously observed rates (Fig. 3 versus Fig. S2). Therefore, methemoglobin reduction cannot account for the metabolic effects observed in pervanadate-treated samples.

Discussion

Considerable indirect evidence has accumulated in support of the GE–band 3 model (31, 32). However, the practical challenge of disrupting the GE–band 3 complex and measuring metabolic fluxes in intact cells has prevented the GE–band 3 model from being convincingly demonstrated. In this study, we took advantage of a ^{1}H-^{13}C NMR strategy for measuring metabolic fluxes in intact cells (Fig. 1) to investigate the metabolic consequences of disrupting the GE–band 3 complex under physiologically relevant conditions.

The GE–band 3 model (Fig. 4) predicts that pervanadate-induced disruption of the GE–band 3 complex will release catalytic inhibition of the GEs and thereby stimulate glycolytic flux and reduce PPP flux. Indeed, oxygenated pervanadate-treated samples had 45% higher glycolytic fluxes and 66% lower pentose shunt fluxes than controls. Moreover, pervanadate-induced metabolic alterations were specific to oxygenated samples: metabolic fluxes of deoxygenated samples did not differ significantly between controls and pervanadate-treated samples. This result was expected because the GE–band 3 complex forms only under oxygenated conditions. The asymmetric effects of pervanadate on oxygenated, but not deoxygenated, samples resulted in an oxygen-insensitive metabolic condition. In contrast, untreated controls were highly responsive to alterations in oxygen tension.

Although both the glycolytic and PPP flux data support the GE–band 3 model, pervanadate has several known side effects that must be addressed. Pervanadate and orthovanadate inhibit several GEs (33). However, our data indicate that that the pervanadate concentrations used in this study were insufficient to influence glycolytic and pentose shunt fluxes directly. Direct inhibition of GEs by pervanadate lowers glycolytic flux (34), whereas we observed increased glycolytic flux in oxygenated samples treated with pervanadate. In addition, direct inhibition of GEs by pervanadate is an oxygen-independent phenomenon,

Table 1. Metabolic fluxes in isotopically labeled red cells measured by ^{1}H NMR and ^{1}H-^{13}C NMR

Metabolite	Control O_2	Control argon	Pervanadate O_2	Pervanadate argon	Methylene blue (O_2)
^{1}H NMR					
Glucose	0.62 ± 0.04	0.89 ± 0.05	1.12 ± 0.08	0.86 ± 0.02	0.67 ± 0.37
Lactate	1.55 ± 0.07	2.14 ± 0.02	2.9 ± 0.03	2.09 ± 0.05	1.45 ± 0.05
PC*	0.06 ± 0.01	0.03 ± 0.005	0.03 ± 0.0001	0.02 ± 0.01	0.21 ± 0.03
^{1}H-^{13}C NMR					
Glucose	0.86 ± 0.03	1.09 ± 0.06	1.14 ± 0.02	0.99 ± 0.03	
2,3-BPG	0.91 ± 0.04	1.58 ± 0.01	†	†	
Pyruvate‡	0.1 ± 0.01	0.03 ± 0.003	0.13 ± 0.01	0.1 ± 0.03	
Lactate	1.81 ± 0.04	2.84 ± 0.02	3.28 ± 0.02	2.53 ± 0.04	
Alanine‡	0.02 ± 0.0004	0.02 ± 0.001	0.06 ± 0.01	0.03 ± 0.002	
Δ pH	−0.08 ± 0.02	−0.12 ± 0.02	−0.12 ± 0.01	−0.11 ± 0.003	

Data are expressed as mean ± SD in μmol/h per mL RBC. Pentose shunt and general flux studies were conducted on independent pools of blood. In pentose activity studies, samples were labeled with 2C-^{13}C glucose and analyzed by ^{1}H NMR. In general flux studies, samples were labeled with U-^{13}C glucose and analyzed by ^{1}H-^{13}C NMR.

*PC expresses the fraction of incoming glucose used to produce pentose-derived glyceraldehyde-3-phosphate; metabolic fluxes for various points in the pentose shunt can be calculated by multiplying PC by the glucose uptake rate and adjusting for the appropriate stochimetry.

†No 2,3-BPG production was observed in pervanadate-treated RBCs.

‡Rates of pyruvate and alanine production include extracellular accumulation of these metabolites.

whereas the pervanadate-induced metabolic alterations observed in this study selectively affected oxygenated erythrocytes. Moreover, the pervanadate concentrations used in this study have been shown to have little effect on GE activities in vitro (35). Thus, we conclude that any direct inhibitory effects of pervanadate in this study were secondary to pervanadate-induced disruption of the GE–band 3 complex.

The complete absence of 2,3-BPG and the elevated pyruvate/alanine production we observed in pervanadate-treated samples are band 3-independent effects of pervanadate that have been reported elsewhere (27). The disappearance of 2,3-BPG and elevated pyruvate production are both thought to originate from pervanadate-induced stimulation of the phosphatase activity of bisphosphoglycerate mutase (27). In contrast to previous reports, which have implicated 2,3-BPG in glycolytic regulation (36), our data show no correlation between 2,3-BPG levels and glycolytic fluxes. Under deoxygenated conditions, we observed nearly identical fluxes between untreated controls and pervanadate-treated samples. This finding indicates that pervanadate-induced alterations in 2,3-BPG concentrations did not significantly alter the observed metabolic fluxes.

Another side effect of pervanadate that could influence glycolytic and pentose shunt fluxes relates to its activity as an oxidizing agent. Two of the most conspicuous metabolic effects of oxidation in erythrocytes are increased PPP flux and elevated NADH-dependent methemoglobin reductase activity. However, we observed a 66% decrease in PPP activity of pervanadate-treated samples and incubating samples in carbon monoxide, an inhibitor of methemoglobin formation, had no significant effect on glycolytic activity (Fig. S2). Although the elevated pyruvate/alanine production we observed in pervanadate-treated samples could be attributed to methemoglobin reductase activity, pervanadate-induced pyruvate production was only 5% of the total carbon output and has been previously attributed to 2,3-BPG degradation (27). The low production of pyruvate/alanine relative to total carbon output, negligible effects of carbon monoxide, and lack of a substantial PPP response argue that pervanadate-induced oxidation was relatively minor in this study.

In summary, our findings provide direct evidence for in vivo regulation of oxygen-dependent metabolic flux via the formation and dissociation of the GE–band 3 complex. Pervanadate-induced disruption of the GE–band 3 interaction in intact cells elicited glycolytic and pentose shunt fluxes similar to those found in deoxygenated erythrocytes. Samples that were treated with pervanadate were unable to respond to changes in oxygen tension, whereas untreated controls were highly responsive. Although pervanadate has several known metabolic side effects, these side effects do not appear to be responsible for our results. In contrast, all of the observed glycolytic and pentose shunt flux data were consistent with the GE–band 3 model. These findings suggest that the GE–band 3 complex plays a direct role in regulating oxygen-dependent changes in glycolytic and pentose shunt fluxes of intact erythrocytes.

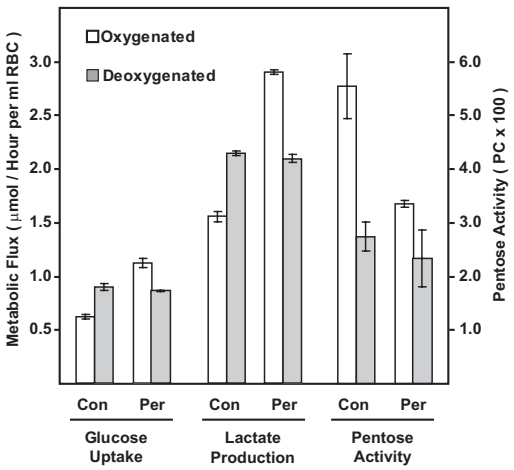

Fig. 3. Rates of glucose consumption, lactate production, and pentose shunt activity (PC) observed in untreated (Con) and pervanadate-treated (Per) RBCs. Empty bars indicate oxygenated samples, filled bars indicate deoxygenated samples, and error bars show standard error.

Materials and Methods

Preparation of RBCs for Metabolic Studies. Fresh blood was collected by venipuncture from healthy human volunteers (n = 6), and erythrocytes from each donor were isolated and washed three times in isotonic Hepes buffer (Table S1). Washed erythrocytes were pooled and resuspended at 20% hematocrit in Hepes buffer containing 20 IU/mL penicillin/streptomycin, after which separate aliquots of the suspension were treated as follows. To stimulate phosphorylation of band 3, erythrocytes were incubated at 37 °C for 30 min with 0.5 mM pervanadate (premixed final concentration of 1.5 mM

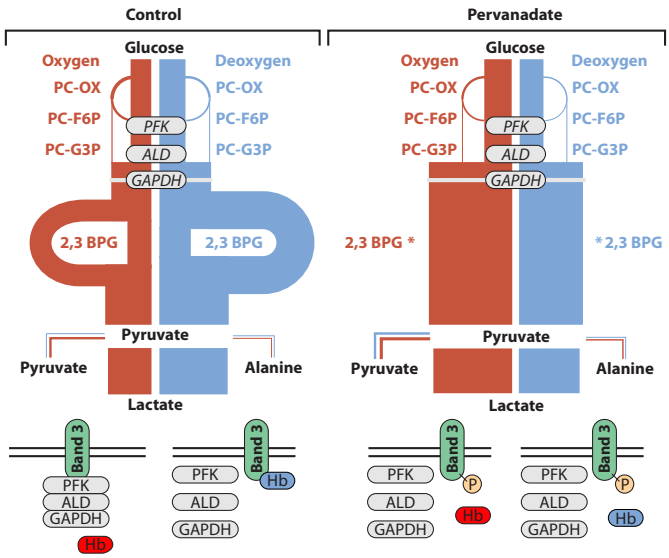

Fig. 4. Metabolic fluxes in RBCs as measured by ^{1}H and ^{1}H-^{13}C NMR. Line widths are proportional to measured fluxes where red lines indicate oxygenated and blue lines indicate deoxygenated conditions. Metabolites used to estimate flux are shown in bold, and the status of the GE–band 3 complex is denoted below each condition. *, No 2,3-BPG production was observed in pervanadate-treated RBCs. PC-OX, flux through the oxidative branch of the PPP; PC-F6P, pentose shunt-derived fructose-6-phosphate; PC-G3P, pentose shunt-derived PC.

hydrogen peroxide and 0.5 mM sodium orthovanadate) via established methods (37). For maximal stimulation of pentose phosphate shunt activity, a separate aliquot of cells was similarly treated with 6.7 μM methylene blue (18–21). For measurement of metabolism in control cells, a third suspension was treated with the same volume of Hepes buffer and then incubated similarly.

Deoxygenated RBCs were prepared by placing small volumes of RBC suspensions in high-volume containers (e.g., 20 mL of suspension in a 250-mL plastic bottle). Containers were fitted with rubber septa, placed on their sides, and gently agitated on a rocking table to maximize the exposed surface area of the suspensions. The agitating suspensions were deoxygenated for 2 h under a continuous stream of humidified argon. All red cell preparations, except the 30-min incubation required for pervanadate-induced phosphorylation of band 3, were conducted in a 4 °C cold room to minimize metabolic activity.

Isotopic Labeling. We used two isotope-based strategies for measuring metabolic flux. PPP activity was calculated from the steady-state positional isotopic enrichment of lactate produced by cells incubated with 5 mM 2-^{13}C-glucose (Isotec 310794). Although this strategy is a well-established method for calculating pentose shunt activity (18, 21), the resulting mixture of isotopomers complicates flux analysis in other pathways. For general metabolic analyses, including measurements of glucose uptake, lactate production, and flux through the 2,3-BPG shunt, we incubated cells with 5 mM U-^{13}C-glucose (Isotec 389374) and monitored the resulting concentration of ^{13}C-labeled metabolites over time. For general flux analysis, washed RBC pools containing 5 mM U-^{13}C-glucose were split into 12 samples consisting of control (oxygenated n = 3; deoxygenated n = 3) and pervanadate-treated samples (oxygenated n = 3; deoxygenated n = 3). At time 0, RBC suspensions were transferred from 4 °C to a 37 °C warm room. Aliquots (1 mL) of each sample were then harvested after 0, 1.5, 3, 6, and 12 h of incubation. Each aliquot was flash-frozen in liquid nitrogen and stored at −80 °C until sample extraction. Sample preparation methods for PPP activity experiments were the same as those used for the general flux studies with the exceptions that cells were incubated with 2-^{13}C-glucose and methylene blue-treated RBC suspensions (n = 3) were added as an additional control.

Sample Extraction and Preparation of Standards. Isotopically labeled samples were suspended in a boiling water bath for 7.5 min to lyse cells and halt enzymatic activity. Boiled lysates were spun at 16,000 × g to pellet cellular debris, and an 800-μL aliquot of each supernatant was dried in a SpeedVac Concentrator (Thermo Scientific). Each resulting metabolite residue was suspended in 800 μL of NMR analytical solution A [D_2O containing 500 μM NaN_3 and 500 μM 4,4-dimethyl-4-silapentane-1-sulfonic acid (DSS)]. Concentration reference solutions containing equimolar (at 2, 5, and 10 mM) glucose, lactate, 2,3-BPG, pyruvate, and alanine were prepared from weighed pure standards (Sigma) dissolved in Hepes-buffered saline (Table S1) prepared in D_2O. Each of the three reference solutions was titrated to an observed glass electrode pH of 7.40 by adding deuterated acid (DCl) or base (NaOD) as needed.

NMR Spectroscopy. NMR spectroscopy was conducted at the National Magnetic Resonance Facility at Madison, WI. 1D ^{1}H and 2D ^{1}H-^{13}C heteronuclear single quantum coherence (HSQC) spectra were collected on a Varian 600-MHz spectrometer equipped with a cryogenic probe. The pulse sequence used to collect ^{1}H NMR spectra consisted of a 1-s initial delay followed by a 90° pulse and a 2-s acquisition time (32,000 data points). Each ^{1}H spectrum was collected in four transients with four steady-state transients. Sensitivity-enhanced ^{1}H-^{13}C HSQC spectra were collected in four transients with 16 steady-state transients, 256 increments, a carbon spectral width of 70 ppm, an acquisition time of 300 ms (3,000 data points), and an initial delay of 1 s. 1D and 2D time-domain datasets were Fourier-transformed, phased, and chemical shift-referenced to DSS. HSQC spectra were processed with a shifted exponential sine bell widow function in both the direct and indirect dimensions. All data processing was done automatically by using custom nmrDraw (38) scripts written in-house.

Assigning Metabolites and Calculating Concentrations. We have recently developed methods for identifying (39) and accurately quantifying (40) metabolites in complex solutions by using multidimensional ^{1}H-^{13}C NMR. These methods were developed to mitigate the significant disadvantages associated with 1D NMR analyses of unfractionated biological extracts. Historically, metabolic flux analyses have primarily relied on 1D NMR (18, 21, 41–43). The use of this technique has limited both the number of metabolites that can be monitored and the quantitative reliability of experiments (40). The methods presented here are a metabolic flux adaptation of our fast metabolite quantification strategy (40) and can be adapted to any ^{13}C-based metabolic flux study.

Metabolites observed in ^{1}H-^{13}C NMR spectra were identified by comparing peak lists from experimental spectra to peak lists from spectra of model compounds collected by the Madison Metabolomics Consortium (39). All assignments were verified by overlaying spectra of pure standards over the spectrum of a representative extract. Peak intensities (area for 1D spectra; peak height for 2D spectra) of dispersed signals from each metabolite (Fig. 1) were normalized to the average Hepes signal to minimize error associated with sample handling. NMR spectra of three equimolar mixtures of pure standards (2, 5, and 10 mM for each metabolite) were used to generate calibration curves for relating observed metabolite intensities to molar concentrations. Metabolite signals observed in the RBC extracts were then quantified by using the regression coefficients from the calibration curves.

Determination of Sample pH by NMR. The ^{1}H NMR chemical shifts of several Hepes signals are sensitive to pH and thus can be used as an internal pH indicator. Chemical shifts of Hepes were measured in each sample by ^{1}H-^{13}C HSQC (Fig. 1) and were converted to pH by fitting a titration curve to the observed shifts (Fig. S3). The Hepes titration curve was generated from samples of the Hepes-buffered saline solution (Table S1) prepared in D_2O and hand-titrated to uncorrected glass electrode readings ranging from 5.5 to 10.5. NMR spectra were collected at the National Magnetic Resonance Facility at Madison.

Calculating Pentose Shunt Flux. Several publications (18, 21) discuss the methods for calculating pentose shunt flux from differential isotopic enrichment in the C2 and C3 positions of lactate after a pulse with 2-^{13}C-glucose. Briefly, isotopic enrichment in the C3 position of lactate is indicative of pentose shunt activity, whereas C2 enrichment is indicative of glycolytic flux. The fraction of incoming glucose used to produce pentose-derived glyceraldehyde-3-phosphate (PC) can be calculated from ^{13}C enrichment in the C3 and C2 positions of lactate by using a model initially developed for radioisotope analyses (44) that has since been modified for NMR (18, 21): $C3_{lactate}/C2_{lactate}$ = 2PC/(1 + 2PC). Metabolic flux through various parts of the PPP can then be calculated by adjusting PC for stoichiometry and glucose uptake (flux through the oxidative branch of the pentose shunt = [3 × PC × glucose consumption], pentose shunt-derived fructose-6-phosphate = [2 × PC × glucose consumption], pentose shunt-derived glyceraldehyde-3-phosphate = [PC × glucose consumption], and glycolytic flux = [(1 − PC) × glucose consumption]).

Our method for determining ^{13}C enrichment differs slightly from that

BIOCHEMISTRY

presented by Delgado et al. (18). As in Delgado et al.'s work, we measured isotopic enrichment from ^{13}C coupling detected by ^{1}H NMR. However, Delgado et al. measured enrichment in both the C2 and C3 positions of lactate from the methyl signal of lactate. This approach requires curve fitting to deconvolve the overlapped signals of unlabeled and 2-^{13}C lactate. To avoid curve fitting, we measured C2 enrichment directly from the dispersed methine signal of lactate. All other calculations, including the correction for naturally occurring ^{13}C, were carried out as described by Delgado et al.

Regression Analyses and Statistics. Rates of glucose consumption, lactate production, and flux through 2,3-BPG were based on linear regression of U-^{13}C metabolite concentrations as a function of time. Glucose consumption and lactate production estimates were based on all of the time points. Isotopic labeling kinetics in 2,3-BPG are nonlinear because 2,3-BPG is a pathway intermediate and steady-state concentrations of 2,3-BPG are affected by changes in pH (4). Consequently, 2,3-BPG flux estimates were based on the initial labeling rates observed between the 0- and 1.5-h time points. Standard deviations of the labeling kinetics reflect variation of regression coefficients between sample replicates. All of the *P* values presented are derived from a two-tailed equal variance *t* test.

ACKNOWLEDGMENTS. We thank Adam Steinberg for creating the RBC metabolic pathway summary figure. This work was supported by National Institutes of Health Grants R21 DK070297, GM24417, and P41 RR02301. I.A.L. was the recipient of National Human Genome Research Institute Fellowship 1T32HG002760. NMR data were collected at the National Magnetic Resonance Facility at Madison, which is funded by National Institutes of Health Grants P41 RR02301 and P41 GM GM66326.

1. Uthman E (1998) *Understanding Anemia* (Univ Press of Mississippi, Jackson).
2. Potter RF, Groom AC (1983) Capillary diameter and geometry in cardiac and skeletal muscle studied by means of corrosion casts. *Microvasc Res* 25:68–84.
3. Johnson RM (1994) Membrane stress increases cation permeability in red cells. *Biophys J* 67:1876–1881.
4. Mulquiney PJ, Kuchel PW (1999) Model of 2,3-bisphosphoglycerate metabolism in the human erythrocyte based on detailed enzyme kinetic equations: Computer simulation and metabolic control analysis. *Biochem J* 342:597–604.
5. Mulquiney PJ, Kuchel PW (1999) Model of 2,3-bisphosphoglycerate metabolism in the human erythrocyte based on detailed enzyme kinetic equations: Equations and parameter refinement. *Biochem J* 342:581–596.
6. Mulquiney PJ, Bubb WA, Kuchel PW (1999) Model of 2,3-bisphosphoglycerate metabolism in the human erythrocyte based on detailed enzyme kinetic equations: In vivo kinetic characterization of 2,3-bisphosphoglycerate synthase/phosphatase using 13C and 31P NMR. *Biochem J* 342:567–580.
7. Hamasaki N, Asakura T, Minakami S (1970) Effect of oxygen tension on glycolysis in human erythrocytes. *J Biochem* 68:157–161.
8. Rapoprot I, Berger H, Rapoport SM, Elsner R, Gerber G (1976) Response of the glycolysis of human erythrocytes to the transition from the oxygenated to the deoxygenated state at constant intracellular pH. *Biochim Biophys Acta* 428:193–204.
9. Jensen FB (2004) Red blood cell pH, the Bohr effect, and other oxygenation-linked phenomena in blood O_2 and CO_2 transport. *Acta Physiol Scand* 182:215–227.
10. Jenkins JD, Kezdy FJ, Steck TL (1985) Mode of interaction of phosphofructokinase with the erythrocyte membrane. *J Biol Chem* 260:10426–10433.
11. Murthy SN, Liu T, Kaul RK, Kohler H, Steck TL (1981) The aldolase-binding site of the human erythrocyte membrane is at the NH_2 terminus of band 3. *J Biol Chem* 256:11203–11208.
12. Tsai IH, Murthy SN, Steck TL (1982) Effect of red cell membrane binding on the catalytic activity of glyceraldehyde-3-phosphate dehydrogenase. *J Biol Chem* 257:1438–1442.
13. Rogalski AA, Steck TL, Waseem A (1989) Association of glyceraldehyde-3-phosphate dehydrogenase with the plasma membrane of the intact human red blood cell. *J Biol Chem* 264:6438–6446.
14. Maretzki D, Reimann B, Rapoport SM (1989) A reappraisal of the binding of cytosolic enzymes to erythrocyte membranes. *Trends Biochem Sci* 14:93–96.
15. Campanella ME, Chu H, Low PS (2005) Assembly and regulation of a glycolytic enzyme complex on the human erythrocyte membrane. *Proc Natl Acad Sci USA* 102:2402–2407.
16. Campanella ME, et al. (2008) Characterization of glycolytic enzyme interactions with murine erythrocyte membranes in wild-type and membrane protein knockout mice. *Blood* 112:3900–3906.
17. Chu H, Breite A, Ciraolo P, Franco RS, Low PS (2008) Characterization of the deoxyhemoglobin binding site on human erythrocyte band 3: Implications for O_2 regulation of erythrocyte properties. *Blood* 111:932–938.
18. Delgado TC, Castro MM, Geraldes CF, Jones JG (2004) Quantitation of erythrocyte pentose pathway flux with [2–13C]glucose and 1H NMR analysis of the lactate methyl signal. *Magn Reson Med* 51:1283–1286.
19. Messana I, et al. (1996) Human erythrocyte metabolism is modulated by the O_2-linked transition of hemoglobin. *FEBS Lett* 390:25–28.
20. Murphy JR (1960) Erythrocyte metabolism. II. Glucose metabolism and pathways. *J Lab Clin Med* 55:286–302.
21. Schrader MC, Eskey CJ, Simplaceanu V, Ho C (1993) A carbon-13 nuclear magnetic resonance investigation of the metabolic fluxes associated with glucose metabolism in human erythrocytes. *Biochim Biophys Acta* 1182:162–178.
22. De Rosa MC, Alinovi CC, Galtieri A, Russo A, Giardina B (2008) Allosteric properties of hemoglobin and the plasma membrane of the erythrocyte: New insights in gas transport and metabolic modulation. *IUBMB Life* 60:87–93.
23. Van Dort HM, Moriyama R, Low PS (1998) Effect of band 3 subunit equilibrium on the kinetics and affinity of ankyrin binding to erythrocyte membrane vesicles. *J Biol Chem* 273:14819–14826.
24. Kinoshita A, et al. (2007) Roles of hemoglobin allostery in hypoxia-induced metabolic alterations in erythrocytes: Simulation and its verification by metabolome analysis. *J Biol Chem* 282:10731–10741.
25. Low PS, et al. (1987) Tyrosine phosphorylation of band 3 inhibits peripheral protein binding. *J Biol Chem* 262:4592–4596.
26. Yannoukakos D, et al. (1991) Three regions of erythrocyte band 3 protein are phosphorylated on tyrosines: Characterization of the phosphorylation sites by solid-phase sequencing combined with capillary electrophoresis. *Biochim Biophys Acta* 1066:70–76.
27. Ninfali P, Accorsi A, Fazi A, Palma F, Fornaini G (1983) Vanadate affects glucose metabolism of human erythrocytes. *Arch Biochem Biophys* 226:441–447.
28. Thorburn DR, Kuchel PW (1985) Regulation of the human-erythrocyte hexose-monophosphate shunt under conditions of oxidative stress. A study using NMR spectroscopy, a kinetic isotope effect, a reconstituted system and computer simulation. *Eur J Biochem* 150:371–386.
29. Manuel y Keenoy B, et al. (1991) Generation of ^{3}HOH from D-[6–3H]glucose by erythrocytes: Role of pyruvate alanine interconversion. *Biochem Med Metab Biol* 46:59–74.
30. Kosaka H, Tyuma I, Imaizumi K (1983) Mechanism of autocatalytic oxidation of oxyhemoglobin by nitrite. *Biomed Biochim Acta* 42:S144–S148.
31. Low PS, Rathinavelu P, Harrison ML (1993) Regulation of glycolysis via reversible enzyme binding to the membrane protein, band 3. *J Biol Chem* 268:14627–14631.
32. Weber RE, et al. (2004) Modulation of red cell glycolysis: Interactions between vertebrate hemoglobins and cytoplasmic domains of band 3 red cell membrane proteins. *Am J Physiol* 287:R454–R464.
33. Simons TJ (1979) Vanadate: A new tool for biologists. *Nature* 281:337–338.
34. Benabe JE, Echegoyen LA, Pastrana B, Martinez-Maldonado M (1987) Mechanism of inhibition of glycolysis by vanadate. *J Biol Chem* 262:9555–9560.
35. Climent F, Bartrons R, Pons G, Carreras J (1981) Effect of vanadate on phosphoryl transfer enzymes involved in glucose metabolism. *Biochem Biophys Res Commun* 101:570–576.
36. Duhm J (1975) Glycolysis in human erythrocytes containing elevated concentrations of 2, 3-P2-glycerate. *Biochim Biophys Acta* 385:68–80.
37. Harrison ML, Rathinavelu P, Arese P, Geahlen RL, Low PS (1991) Role of band 3 tyrosine phosphorylation in the regulation of erythrocyte glycolysis. *J Biol Chem* 266:4106–4111.
38. Delaglio F, et al. (1995) NMRPipe: A multidimensional spectral processing system based on UNIX pipes. *J Biomol NMR* 6:277–293.
39. Cui Q, et al. (2008) Metabolite identification via the Madison Metabolomics Consortium Database. *Nat Biotechnol* 26:162–164.
40. Lewis IA, et al. (2007) Method for determining molar concentrations of metabolites in complex solutions from two-dimensional ^{1}H-^{13}C NMR spectra. *Anal Chem* 79:9385–9390.
41. Shulman RG, Rothman DL (2001) C-13 NMR of intermediary metabolism: Implications for systemic physiology. *Annu Rev Physiol* 63:15–48.
42. Berthon HA, Bubb WA, Kuchel PW (1993) 13C n.m.r. isotopomer and computer-simulation studies of the nonoxidative pentose phosphate pathway of human erythrocytes. *Biochem J* 296:379–387.
43. McIntyre LM, Thorburn DR, Bubb WA, Kuchel PW (1989) Comparison of computer simulations of the F-type and L-type nonoxidative hexose monophosphate shunts with 31P-NMR experimental data from human erythrocytes. *Eur J Biochem* 180:399–420.
44. Katz J, Wood HG (1960) The use of glucose-C14 for the evaluation of the pathways of glucose metabolism. *J Biol Chem* 235:2165–2177.